neuron responded at the second syllable, and the response was suppressed by deletion of the first or second syllable.
13. D. Margoliash, *J. Neurosci.* **3**, 1039 (1983); D. Margoliash, E. S. Fortune, *J. Neurosci.* **12**, 4309 (1992).
14. We gathered sufficient data from 14 neurons (from three birds) to permit quantitative comparisons between ongoing discharge and singing. Interspike interval histograms of the ongoing discharge of RA neurons during sleep are bimodal; the longer interval peak is related to nonbursting activity. Thus, bursts were defined as continuous sequences of interspike intervals falling outside of the normal (nonbursting) distribution of intervals.
15. Two tests of significance were devised. For each neuron, a distance was computed between each ongoing burst and the exemplar stretch of activity during singing. Each best match (lowest distance) was tested for significance by using a bootstrap procedure that assessed the probability of occurrence of the exact sequence of intervals observed in the burst. In the second test, for the one bird with the greatest number of recordings, we also compared each neuron's ongoing discharges during sleep with the premotor data from other neurons. For seven out of eight neurons, there were more matches with the neuron's own premotor data than with the premotor data from the other neurons. The same neuron failed to achieve significance in both tests.
16. The procedures for identifying bursts in ongoing activity, matching bursts to premotor activity, and assessing the significance of the matches are described in detail on *Science* Online (*24*).
17. M. Konishi, *Z. Tierpsychol.* **22**, 770 (1965).
18. C. E. Carr, W. Heiligenberg, G. J. Rose, *J. Neurosci.* **6**, 107 (1986); *J. Neurosci.* **6**, 1372 (1986); A. Moiseff, M. Konishi, *J. Neurosci.* **1**, 40 (1981); C. E. Carr, M. Konishi, *J. Neurosci.* **10**, 3227 (1990); G. Laurent, M. Wehr, H. Davidowitz, *J. Neurosci.* **16**, 3837 (1996); R. C. deCharms, M. M. Merzenich, *Nature* **381**, 610 (1996); A. K. Engel, P. R. Roelfsema, P. Fries, M. Brecht, W. Singer, *Cereb. Cortex* **7**, 571 (1997); Y. Prut *et al.*, *J. Neurophysiol.* **79**, 2857 (1998).
19. E. T. Vu, M. E. Mazurek, Y.-C. Kuo, *J. Neurosci.* **14**, 6924 (1994).
20. S. W. Bottjer, F. Johnson, *J. Neurobiol.* **33**, 602 (1997).
21. M. Luo, D. J. Perkel, *J. Neurosci.* **19**, 6700 (1999).
22. G. E. Hinton, P. Dayan, B. J. Frey, R. M. Neal, *Science* **268**, 1158 (1995).
23. G. Buzsáki, *Neuroscience* **31**, 551 (1989); M. A. Wilson, B. L. McNaughton, *Science* **265**, 676 (1994); W. E. Skaggs, B. L. McNaughton, *Science* **271**, 1870 (1996); Z. Nádasdy, H. Hirase, A. Czurkó, J. Csicsvari, G. Buzsáki, *J. Neurosci.* **19**, 9497 (1999).
24. Supplemental data are available at www.sciencemag.org/feature/data/1051099.shl.
25. We thank T. Q. Gentner, J.-M. Ramirez, P. S. Ulinski, and especially two anonymous reviewers for valuable comments on the manuscript. This work was supported by grants from the NIH (MH59831 and MH60276) to D.M. and (MH11615) to A.S.D.

6 April 2000; accepted 8 September 2000

Structure of Murine CTLA-4 and Its Role in Modulating T Cell Responsiveness

David A. Ostrov,[1,2] Wuxian Shi,[2] Jean-Claude D. Schwartz,[1] Steven C. Almo,[2]* Stanley G. Nathenson[1,3]*

The effective regulation of T cell responses is dependent on opposing signals transmitted through two related cell-surface receptors, CD28 and cytotoxic T lymphocyte–associated antigen 4 (CTLA-4). Dimerization of CTLA-4 is required for the formation of high-avidity complexes with B7 ligands and for transmission of signals that attenuate T cell activation. We determined the crystal structure of the extracellular portion of CTLA-4 to 2.0 angstrom resolution. CTLA-4 belongs to the immunoglobulin superfamily and displays a strand topology similar to Vα domains, with an unusual mode of dimerization that places the B7 binding sites distal to the dimerization interface. This organization allows each CTLA-4 dimer to bind two bivalent B7 molecules and suggests that a periodic arrangement of these components within the immunological synapse may contribute to the regulation of T cell responsiveness.

T cell–dependent immune processes require cell-surface interactions that mediate the initiation, modulation, and the ultimate course of the response. The specificity of T cell recognition is determined by the engagement of the T cell receptor (TCR) on T cells with cognate peptide–major histocompatibility complex (MHC) complexes presented by antigen-presenting cells (APCs) (*1*, *2*). Additional signals are required to sustain and enhance T cell activity, the most important of which is provided by the engagement of CD28 on T cells with its ligands B7-1 (CD80) and B7-2 (CD86) on APCs (*3*, *4*). In contrast, the interaction of B7 isoforms with CTLA-4, a CD28 homolog (31% identity), provides inhibitory signals required for down-regulation of the response (*5*).

Unlike CD28, which is expressed on resting T cells, CTLA-4 is not detected on the cell surface until 24 hours after activation, peaking at 36 to 48 hours after activation (*6*). In addition, CTLA-4 exhibits an affinity for the B7 isoforms that is 10 to 100 times that for CD28 (*7*). On the basis of these differences in expression patterns and affinities, it is likely that CTLA-4 directly competes with CD28 for binding B7 and also directs the assembly of inhibitory signaling complexes that lead to quiescence or anergy (*8*). Consistent with the inhibitory role of CTLA-4, mice deficient in CTLA-4 die as a consequence of unchecked polyclonal T cell expansion, which results in fatal lymphoproliferative disorders (*9*). Thus, the balance between the opposing signals elicited by CD28 and CTLA-4 is central to the regulation of T cell responsiveness and homeostasis (*10*).

Because of its dominant role in modulating T cell activity, CTLA-4 has received considerable attention as a therapeutic agent (*11*). The soluble CTLA-4–immunoglobulin (CTLA-4–Ig) fusion protein acts as an inhibitor of CD28-B7 costimulation and has specific inhibitory effects in animal models of autoimmunity, transplant rejection, asthma, and allergy (*3*, *12*). The efficacy of CTLA-4–Ig treatment of human disease has been demonstrated in clinical trials on patients with psoriasis vulgaris (*13*). This approach may well extend to a variety of T cell–mediated diseases including autoimmune diabetes, rheumatoid arthritis, systemic lupus erythematosus, and graft-versus-host disease (*13*). In contrast to strategies that interfere with the CD28-B7 association, reagents that interfere with the CTLA-4–B7 interaction intensify specific T cell responses. For example, blocking antibodies directed against CTLA-4 enhance rejection of preestablished tumors and protect against secondary challenge in animal models of prostate cancer and colon carcinoma (*14*).

The structure of the soluble extracellular domain of murine CTLA-4 (*15*) revealed two independent copies of the CTLA-4 dimer in the asymmetric unit of the crystal (Fig. 1, A and B, and Table 1) (*16*). The CTLA-4 monomer is a two-layer β-sandwich that exhibits the chain topology found in the immunoglobulin variable domains (Fig. 1A) (*17*). The front and back sheets, composed of strands A′GFCC′ and ABEDC″, respectively, are connected by two intersheet disulfide bonds. The disulfide bond between the B and F strands is a signature for the immunoglobulin fold; the disulfide bond joining strands C′ and D is unique to the CD28/CTLA-4 family (Fig. 1A) (*17*, *18*).

The nuclear magnetic resonance (NMR) structure of a monomeric form of human CTLA-4 (*18*) shows the same overall topology as the murine homolog, with a root mean square (rms) deviation of 2.4 Å between equivalent Cα atoms. The most significant

[1]Department of Microbiology and Immunology, [2]Department of Biochemistry, [3]Department of Cell Biology, Albert Einstein College of Medicine, Bronx, NY 10461. USA.

*To whom correspondence should be addressed. E-mail: almo@aecom.yu.edu or nathenso@aecom.yu.edu

difference involves the C″ strand, which in the crystal structure is hydrogen-bonded to the ABED sheet, as in Vα domains (Fig. 1A); in the NMR structure this region is defined as a loop and does not interact with either sheet (A′GFCC′ or ABED). Structural alignment (*19*) shows that CTLA-4 is most similar to the Vα and V_H domains present in antigen receptors, with rms deviations of 3.0 and 3.1 Å, respectively (*20*).

The CTLA-4 dimer interface is not formed by the A′GFCC′ sheet (front-to-front packing) as observed in variable (v-type) immunoglobulin dimers, such as VαVβ and V_LV_H heterodimers and CD8 homodimers (*21*). Instead, CTLA-4 exhibits a dimer interface similar to that present in the constant (c-type) family members, such as C_H3 homodimers and C_LC_H1 heterodimers, which involves the BED strands (back-to-back packing) (Fig. 1B) (*22*). Several distinct features of the CTLA-4 monomer are consistent with this unusual dimerization mode: (i) The front sheet of CTLA-4 is flatter than other v-type immunoglobulin domains, precluding a number of contacts critical for front-to-front packing; (ii) CTLA-4 lacks one (C′ strand) of the two β bulges (C′ and G) in the front sheet that are characteristic of front-to-front packing; (iii) the front sheet of CTLA-4 is considerably less hydrophobic than v-type dimers, consistent with its exposure to solvent; (iv) the placement of the C″ strand in CTLA-4 augments the back sheet (strands ABEDC″), contributing six van der Waals contacts to the dimerization interface that are not present in other v-type dimers; and (v) modeling studies show that putative front-to-front packing of CTLA-4 monomers is sterically incompatible with the known binding surface for B7 ligands (*18*).

The CTLA-4 dimer interface is stabilized by four hydrogen bonds, 48 van der Waals contacts, and 15 water-mediated hydrogen bonds, involving a number of residues that are largely conserved among CTLA-4 homologs, including His^{14}, Glu^{22}, Arg^{74}, and Gln^{80} (Fig. 1C). These residues are not conserved in CD28 (Fig. 2), suggesting differences in the dimer interface and/or quaternary organization. The total surface area buried at the CTLA-4 dimer interface is 1597 $Å^2$, which is comparable with the C_LC_H1 (1500 to 2100 $Å^2$) and C_H3C_H3 interfaces (2200 $Å^2$) (*23*). Although CTLA-4 and the c-type immunoglobulin dimers both utilize back-to-back packing, the relative orientation of the monomers within the dimers differs considerably. Superposition of a CTLA-4 monomer with C_H1 would require a 10° to 12° rotation and a 9 to 10 Å translation to align the second CTLA-4 monomer on C_L (*24*). The structure of human B7-1 reveals that the membrane distal domain, which binds CTLA-4, displays the v-type immunoglobulin topology and also homodimerizes via the back face (*25*). The structural similarity

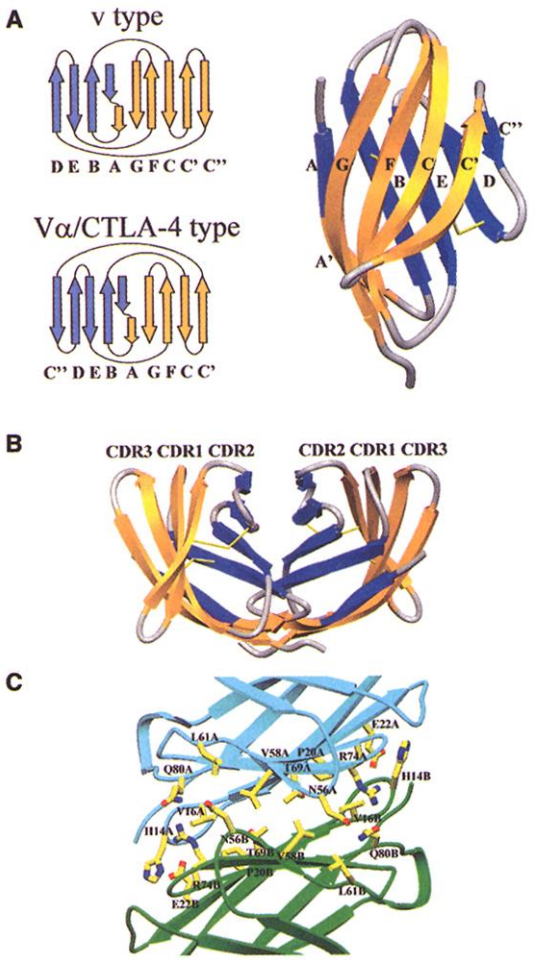

Fig. 1. Structure of CTLA-4. (**A**) On the right, ribbon diagram of the CTLA-4 monomer. The β strands are labeled: A (3 to 6), A′ (7 to 11), B (16 to 24), C (30 to 39), C′ (43 to 53), C″ (56 to 59), D (65 to 70), E (74 to 80), F (87 to 99), and G (103 to 114). The A′GFCC′ (front) and ABEDC″ (back) sheets are shown in gold and blue, respectively. Intersheet disulfide bonds between the B and F strands and between the C′ and D strands are shown in yellow. Inset on the top left shows the strand topology for typical v-type immunoglobulin domains (e.g., V_H, V_L, Vβ). Inset on the bottom left shows the strand topology for Vα domains and CTLA-4 in which the C″ strand is part of the back sheet. (**B**) Ribbon diagram of the CTLA-4 dimer. The CTLA-4 homodimer is oriented with the molecular diad axis situated vertically in the plane of the page. In this orientation, the COOH-termini extend from the bottom of the molecule. The dimer interface is formed primarily by the ABEDC″ (back) sheets, shown in blue. The CDR analogous regions, CDR1 (BC loop), CDR2 (C′C″ loop), and CDR3 (FG loop), form the top surface of the molecule. The distance between the CDR3 analogous regions in the dimer is 47 Å. (**C**) Detailed view of the CTLA-4 dimer interface. The twofold axis of the dimer is perpendicular to the page. The backbones of the CTLA-4 monomers are shown in green and in sky blue. The side chains involved in hydrogen bonding and van der Waals interactions at the dimer interface are displayed (*23*), with C, O, and N atoms depicted in yellow, red, and blue, respectively. Figure 1 was made with the program SETOR (*41*).

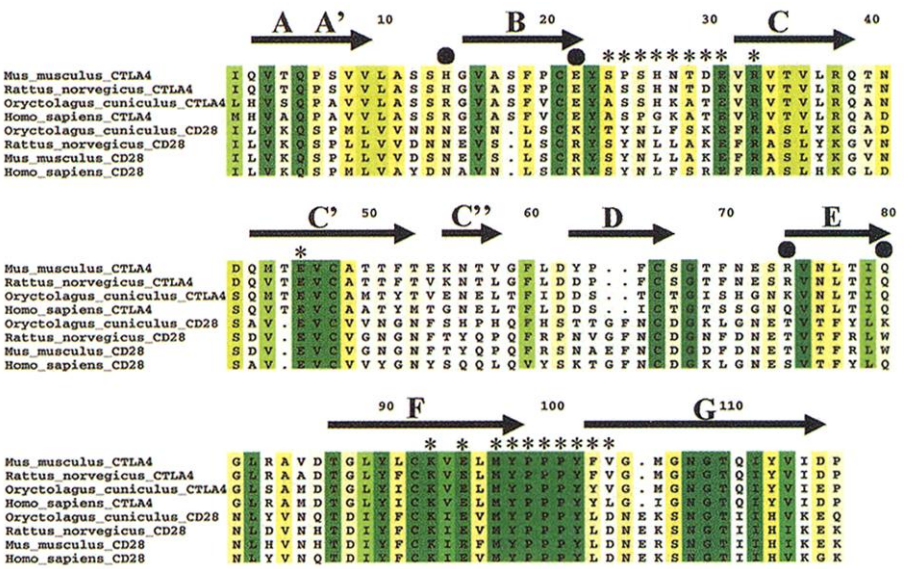

Fig. 2. Sequence alignment of the CTLA-4 and CD28 family (*43*). CTLA-4 and CD28 sequences were aligned with ClustalX (*42*). Positions with 50 to 100% sequence similarity are colored in hues graded from yellow to green. Mutations that affect the binding of CTLA-4 to B7 are labeled "*". Residues contributing to hydrogen bonds at the CTLA-4 dimer interface are indicated with filled circles. The β strands were defined according to the murine CTLA-4 structure. Figure 2 was made with ALSCRIPT (*44*).

within this receptor-ligand pair suggests an evolutionary relationship.

Mutagenesis studies have identified a series of residues involved in B7 binding that cluster to a single surface on CTLA-4, including the FG loop, the BC loop, and residues on the A′GFCC′ face (Arg[33], Thr[35], Leu[37], Glu[46], Thr[51]; Fig. 3C) (*18*, *26*). The FG loop, which is analogous to CDR3 present in immunoglobulins and TCRs, contains the Met[97]TyrProProProTyr[102] sequence motif, which is highly conserved in CTLA-4 and CD28 sequences from different species (Fig. 2) and is critical in mediating the interaction with B7. The unique *cis-trans-cis* conformations of the three consecutive proline residues and their relatively low B factors suggest that these residues play a direct role in binding B7 and are required to maintain the loop in a productive binding conformation. Residues in the BC loop, the region analogous to CDR1, also appear to be determinants of binding affinity, as grafting the CDR1 region of CTLA-4 onto CD28 dramatically increased the binding strength of the chimeric molecule for B7 (*26*). A prominent feature evident on the B7 binding surface of CTLA-4 is a predominantly hydrophobic pocket, approximately 10 Å in diameter and 9 Å deep, formed by residues contributed by the CDR1- and CDR3-like loops. This pocket may con-

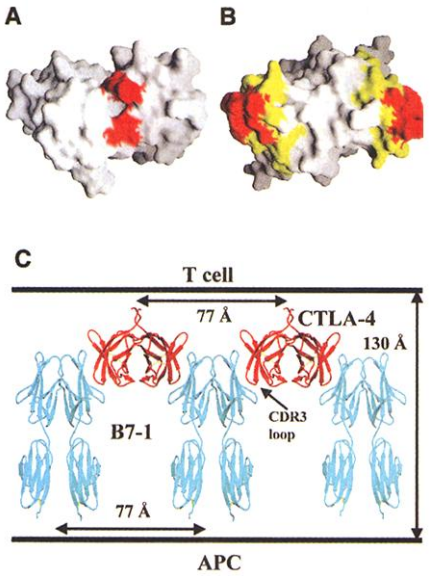

Fig. 3. B7 binding sites on CTLA-4 and placement of CDR3 regions in dimers of immunoglobulin domains. The molecular surfaces of the TCR VαVβ heterodimer (1tcr) and the CTLA-4 homodimer (1dqt) are shown in (**A**) and (**B**), respectively, with the CTLA-4 twofold axis oriented perpendicular to the page. Because of front-to-front packing in the TCR, the CDR3 regions shown in red are juxtaposed at the dimer interface (A), whereas the back-to-back packing present in CTLA-4 positions the CDR3 regions distal to the dimer interface (B). The two B7 binding sites on the CTLA-4 homodimer, as mapped by mutagenesis (*26*), include the FG loop (CDR3) shown in red, the BC loop (CDR1) shown in yellow, and solvent-accessible residues on the A′GFCC′ sheet (Glu[31], Arg[33], Glu[46], Lys[93], Glu[95], Phe[103], and Val[104]), shown in yellow (*18*). In contrast to VαVβ and Fab, which are monovalent for their respective ligands (i.e., peptide-MHC complex and antigen), the placement of ligand binding sites at the extremes of the CTLA-4 dimer suggests that each CTLA-4 monomer may interact with an individual B7 dimer. (A) and (B) were prepared with GRASP (*45*). (**C**) Model of organized interactions between CTLA-4 and B7 dimers in the immunological synapse. CTLA-4 dimers, shown in red, are depicted with their COOH-termini modeled to include the disulfide bond at Cys[120] near the T cell plasma membrane. CTLA-4 was manually docked to B7-1 d1, shown in light blue, to maximize the interaction between residues implicated by site-directed mutagenesis, in particular, CDR3 (Met[97]TyrProProProTyr[102]) of CTLA-4, and a hydrophobic patch on the A′GFCC′C″ face of B7-1 (*25*). Each CTLA-4 dimer is depicted as binding two independent B7 dimers with an intermolecular spacing of approximately 77 Å and an intermembrane distance spanned by the CTLA-4–B7 ligand pair of approximately 100 Å. (C) was made with the program SETOR (*41*).

Table 1. Crystallographic analysis. Native and selenomethionyl-substituted *Mus musculus* CTLA-4 were expressed in *Escherichia coli*. Crystals of CTLA-4 were grown by hanging drop vapor diffusion at 18°C. A portion (2 μl) of a 10 mg/ml protein solution was mixed with 2 μl of crystallization buffer composed of 20% PEG 6000, 2.0 M NaCl, pH 6.5, and equilibrated against a 1-ml reservoir of the same buffer. Diffraction from these crystals is consistent with the space group $P4_32_12$ ($a = b = 112.85$ Å, $c = 102.50$ Å; four monomers in the asymmetric unit, 58% solvent). Crystals were transferred stepwise to cryoprotectant solution containing 20% ethylene glycol in crystallization buffer and flash cooled at 100 K. MAD data were collected at beamline X12C (National Synchrotron Light Source, Brookhaven National Laboratory). Data were recorded at wavelengths of 0.9789, 0.9786, and 0.9500 Å on a Brandeis charge-coupled device detector and reduced with the HKL suite (*34*). The 12 selenium sites were located by direct methods (*35*) and by difference Patterson and cross validation difference Fourier methods implemented in the SOLVE package (*36*). Electron density maps, enhanced with fourfold noncrystallographic averaging and solvent flattening using DM (*37*), allowed 95% of the residues to be traced using the program O (*38*). The model was refined against native data collected on a MAR345 detector at beamline X9B (NSLS, BNL) and subjected to anisotropic and bulk solvent correction, simulated annealing refinement, and individual B-factor refinement using the CNS package (*39*). The final model is of high quality, with 99% of the residues in the most favored and additionally allowed regions (*40*). The rms deviation between related by noncrystallographic symmetry is 0.5 Å.

	Data collection statistics			
Data set	CTLA-4 native	Se edge	Se peak	Se remote
Detector	Mar345	Brandeis CCD	Brandeis CCD	Brandeis CCD
Beamline	X-9B (NSLS)	X-12C (NSLS)	X-12C	X-12C
Resolution (Å)*	2.0 (2.07–2.00)	3.0 (3.05–3.00)	3.0 (3.05–3.00)	3.0 (3.05–3.00)
Wavelength (Å)	0.9789	0.9789	0.9786	0.9500
Reflections:				
Total	301,486	77,098	76,888	74,730
Unique	44,587	13,676	13,669	13,708
$I/\sigma(I)$	36.5 (5.7)	21.0 (9.1)	18.0 (7.3)	23.7 (11.0)
Completeness:	99.4 (95.7)	98.7 (100.0)	98.7 (100.0)	98.5 (100.0)
R_{sym} (%)†	6.2 (36.3)	6.9 (12.7)	8.8 (16.3)	6.8 (11.4)
R_{anom} (%)‡		4.9	6.8	4.3
		Refinement statistics		
Resolution (Å)		20.0–2.0		
R_{cryst} (%)§		20.9		
R_{free} (%)‖		25.4		
Reflections over 2σ:				
For refinement		35,364		
For R_{free}		3,965		
Protein atoms		3,632		
Water molecules		431		
Average B factors (Å^2)				
Protein		31.9		
Water		42.4		
rms deviations from ideal				
Bond lengths (Å)		0.009		
Angles (°)		1.55		
		Ramachandran plot		
Most favored (%)		92.0		
Additionally allowed (%)		7.0		
Generously allowed (%)		1.0		
Disallowed (%)		0.0		

*Values in parentheses are for the highest resolution shell. †$R_{sym} = \Sigma_i | I_{hi} - \langle I_{hi} \rangle | / \Sigma_i | I_{hi} |$, where h specifies unique reflection indices, i indicates symmetry equivalent observations of h. ‡$R_{anom} = \Sigma_h | I_h^+ - I_h^- | / \Sigma_h | I_h^+ + I_h^- |$, where h specifies unique reflection indices. §$R_{cryst} = \Sigma | F_o - F_c | / \Sigma | F_o |$ for all reflections, where F_o and F_c are the observed and calculated structure factors, respectively. ‖R_{free} was calculated against 10% of the reflections removed at random from the refinement.

tact a hydrophobic patch on the membrane distal part of B7-1, including Met^{38}, Trp^{50}, and Tyr^{53}, which are essential for binding to CTLA-4 (*25*).

Certain features of the CTLA-4 dimer, in particular the placement of CDR3, appear to be relevant to its interaction with B7 and the regulation of signaling events at the synapse formed by the T cell–APC interface. As a consequence of the unusual dimerization mode used by CTLA-4, the FG loop (CDR3) is located distal to the dimerization interface (Figs. 1B and 3B). This organization contrasts with other v-type immunoglobulin domains where CDR3 is located proximal to the dimer interface (Fig. 3A), and provides CTLA-4 with the potential for novel ligand-binding interactions. A model of the CTLA-4/B7 complex was generated by manual docking, which maximized the interactions of residues contributing to the binding interface as defined by site-directed mutagenesis (Fig. 3C). This model predicts that the CTLA-4–B7 interface is formed primarily by the front sheets (A′GFCC′) of the respective molecules and buries a total surface area of ~1200 $Å^2$. This packing arrangement is similar to that observed in the structures of the heterophilic CD2/CD58 and homophilic Po-Po complexes that bury 1507 and 984 $Å^2$, respectively (*27*, *28*).

The dimeric organization of both CTLA-4 and B7-1 at the T cell–APC interface is consistent with the formation of a periodic structure, in which each CTLA-4 dimer bridges two B7 molecules, with an interdimer spacing of ~77 Å (Fig. 3C). Steric considerations appear to preclude a bidentate interaction between individual CTLA-4 and B7 dimers. The dimensions of the CTLA-4 and B7 molecules suggest an intermembrane distance of ~100 Å, which is compatible with the linear dimensions of the TCR–peptide/MHC and the CD2-CD58 complexes that measure approximately 130 Å in their maximum dimension (*2*, *27*).

The putative organization of the CTLA-4–B7 complex suggests that in addition to antagonism of CD28 costimulation through competition for B7 by high-avidity CTLA-4 dimers, more elaborate regulatory mechanisms might operate by the recruitment and ordering of intracellular signaling components to the TCR complex in the immunological synapse (*29*, *30*). Initial engagement between T cell and APC results in phosphorylation of the TCR ζ chain, and directs subsequent cytoskeletal events that lead to clustering of the TCR and peptide-MHC complexes within the synapse. As CTLA-4 coimmunoprecipitates with both TCR ζ and SHP-2 phosphatase, the binding of CTLA-4 to B7 in the central region of the synapse could inhibit TCR signaling by directing the SHP-2–mediated dephosphorylation of TCR ζ (*31*–*33*). This physical linkage between CTLA-4 and the TCR complex also suggests that CTLA-4 might direct short-range ordering of signaling components within the central zone of the immunological synapse. Thus, CTLA-4 might function as both a competitor of CD28 function and as an organizing element required for negative signaling within the synapse.

References and Notes

1. C. A. J. Janeway, K. Bottomly, *Semin. Immunol.* **8**, 108 (1996).
2. K. C. Garcia, L. Teyton, I. A. Wilson, *Annu. Rev. Immunol.* **17**, 369 (1999).
3. E. A. Greenfield, K. A. Nguyen, V. K. Kuchroo, *Crit. Rev. Immunol.* **18**, 389 (1998).
4. C. A. Chambers, J. P. Allison, *Curr. Opin. Cell Biol.* **11**, 203 (1999).
5. M. F. Krummel, J. P. Allison, *J. Exp. Med.* **182**, 459 (1995).
6. C. B. Thompson, J. P. Allison, *Immunity* **7**, 445 (1997).
7. P. A. van der Merwe, D. L. Bodian, S. Daenke, P. Linsley, S. J. Davis, *J. Exp. Med.* **185**, 393 (1997).
8. P. S. Linsley, P. Golstein, *Curr. Biol.* **6**, 398 (1996).
9. E. A. Tivol *et al.*, *Immunity* **3**, 541 (1995).
10. J. A. Bluestone, *J. Immunol.* **158**, 1989 (1997).
11. M. H. Sayegh, *J. Clin. Invest.* **103**, 1223 (1999).
12. D. J. Lenschow *et al.*, *Immunity* **5**, 285 (1996).
13. J. R. Abrams *et al.*, *J. Clin. Invest.* **103**, 1243 (1999).
14. E. D. Kwon *et al.*, *Proc. Natl. Acad. Sci. U.S.A.* **94**, 8099 (1997).
15. The extracellular domain of CTLA-4 encompassing residues 1 to 119 was expressed in BL21(DE3), refolded from inclusion bodies, and purified by anion-exchange chromatography.
16. CTLA-4 expressed on the surface of T cells contains at least one N-linked carbohydrate (*7*). Human CTLA-4 expressed in Chinese hamster ovary (CHO) cells is glycosylated on Asn^{76} and Asn^{108}, the equivalents of Asn^{78} and Asn^{110} in murine CTLA-4. The observed crystal structure is not compatible with glycosylation at Asn^{78}, as this would interfere with the formation of the back-to-back dimer interface. This apparent inconsistency is perhaps attributable to differences in the glycosylation properties of T cells and CHO cells. However, the observed dimer is compatable with glycosylation at the solvent exposed Asn^{110}, which resides in the G strand β bulge on the front sheet of murine CTLA-4.
17. P. Bork, L. Holm, C. Sander, *J. Mol. Biol.* **242**, 309 (1994).
18. W. J. Metzler *et al.*, *Nature Struct. Biol.* **4**, 527 (1997).
19. L. Holm, C. Sander, *J. Mol. Biol.* **233**, 123 (1993).
20. Protein structures: TCR, Protein Data Bank (PDB) code 1tcr (*21*); Fab of monoclonal antibody to gp120, 1gc1 [P. D. Kwong *et al.*, *Nature* **393**, 648 (1998)]; Po, 1neu [L. Shapiro, J. P. Doyle, P. Hensley, D. R. Colman, W. A. Hendrickson, *Neuron* **17**, 435 (1996)]; CD8, 1cd8 [D. J. Leahy, R. Axel, W. A. Hendrickson, *Cell* **68**, 1145 (1992)]; CD2, 1hnf [D. L. Bodian, E. Y. Jones, K. Harlos, D. I. Stuart, S. J. Davis, *Structure* **2**, 755 (1994)]; CD58, 1ccz [S. Ikemizu *et al.*, *Proc. Natl. Acad. Sci. U.S.A.* **96**, 4289 (1999)]; CD2d1/CD58d1 complex, 1qa9 (*27*); and CH3, 1fc1 [J. Deisenhofer, *Biochemistry* **20**, 2361 (1981)].
21. K. C. Garcia *et al.*, *Science* **274**, 209 (1996).
22. R. Huber, J. Deisenhofer, P. M. Colman, M. Matsushima, W. Palm, *Nature* **264**, 415 (1976).
23. The van der Waals contacts, hydrogen bond interactions, and buried molecular surfaces were calculated as in (*21*). Other subunit interfaces that occur in the CTLA-4 crystal lattice are significantly less extensive, with buried surface areas of 807 $Å^2$ or less.
24. A V_H domain (1gc1) was first superimposed on one CTLA-4 molecule. The same transformation was then applied to the other CTLA-4 domain to superimpose on the corresponding V_L domain. The additional rotation and translation required to optimize the CTLA-4–V_L superposition describes the domain shift. This procedure is similar to that described in (*21*).
25. S. Ikemizu *et al.*, *Immunity* **12**, 51 (2000).
26. R. J. Peach *et al.*, *J. Exp. Med.* **180**, 20498 (1994).
27. J. H. Wang *et al.*, *Cell* **97**, 791 (1999).
28. L. Shapiro, J. P. Doyle, P. Hensley, D. R. Colman, W. A. Hendrickson, *Neuron* **17**, 435 (1996).
29. M. L. Dustin, A. S. Shaw, *Science* **283**, 649 (1999).
30. A. Grakoui *et al.*, *Science* **285**, 221 (1999).
31. K.-M. Lee *et al.*, *Science* **282**, 2263 (1998).
32. C. Olsson, K. Riebeck, M. Dohlsten, E. Michaëlsson, *J. Biol. Chem.* **274**, 14400 (1999).
33. L. E. M. Marengère *et al.*, *Science* **272**, 1170 (1996).
34. Z. Otwinowski, W. Minor, *Methods Enzymol.* **276**, 307 (1997).
35. C. M. Weeks, R. Miller, *J. Appl. Crystallogr.* **32**, 120 (1999).
36. T. C. Terwilliger, J. Berendzen, *Acta Crystallogr.* **D55**, 849–861, (1999).
37. K. Cowtan, P. Main, *Acta Crystallogr.* **D54**, 487 (1998).
38. T. A. Jones, S. Cowan, J. Y. Zou, M. Kjeldgaard, *Acta Crystallogr.* **A47**, 110 (1991).
39. A. T. Brünger *et al.*, *Acta Crystallogr.* **D54**, 905 (1998).
40. R. A. Laskowski, M. W. MacArthur, D. S. Moss, J. M. Thornton, *J. Appl. Crystallogr.* **26**, 283 (1993).
41. S. V. Evans, *J. Mol. Graphics* **11**, 134 (1993).
42. J. D. Thompson, D. G. Higgins, T. J. Gibson, *Nucleic Acids Res.* **22**, 4673 (1994).
43. Single-letter abbreviations for the amino acid residues are as follows: A, Ala; C, Cys; D, Asp; E, Glu; F, Phe; G, Gly; H, His; I, Ile; K, Lys; L, Leu; M, Met; N, Asn; P, Pro; Q, Gln; R, Arg; S, Ser; T, Thr; V, Val; W, Trp; and Y, Tyr.
44. G. J. Barton, *Methods Enzymol.* **183**, 403 (1990).
45. A. Nicholls, K. A. Sharp, B. Honig, *Proteins Struct. Funct. Genet.* **11**, 281 (1991).

46. Supported by NIH research grants AI07289, CA09173, and AI42970 and Cancer Center support (CORE) grant CA34196. Beamline X9B is supported by RR01633. Beamline X12C is supported by DE-AC02-98CH10886 and RR12408. Coordinates have been deposited at the RCSB structural database (1 dqt). We thank J. Bajorath, P. Linsley, and P. Concannon for insightful comments; S. Sheriff, R. Stanfield, C. Weeks, and D. Jeruzalmi for programs, discussions, and advice; and Z. Dauter and R. Sweet for help with data collection. We especially thank J. Bonnano for computational expertise.

18 June 2000; accepted 11 September 2000